Thermal Science and Engineering Progress 42 (2023) 101935

Contents lists available at ScienceDirect

Thermal Science and Engineering Progress

journal homepage: www.sciencedirect.com/journal/thermal-science-and-engineering-progress

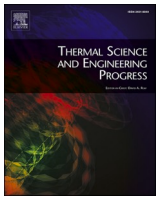

An R1234ze(E) loop heat pipe with flat-plate evaporator for cooling electronic devices

S.C. Zhao [a], Zikang Zhang [a], Runze Zhao [a], Tong Wu [a], Xiaoyu Zhang [b], Z.C. Liu [a], Wei Liu [a,*]

[a] School of Energy and Power Engineering, Huazhong University of Science and Technology, Wuhan 430074, China
[b] Beijing ThermaTech Co., Ltd, Beijing 100096, China

ARTICLE INFO

Keywords:
Loop heat pipe
R1234ze(E)
Flat-plate evaporator
Electronic equipment cooling
Air condenser

ABSTRACT

With the development of high power electronic devices, the failure problem caused by the high temperature must be solved by a reliable cooling solution. A solution for cooling electronic equipment was proposed in this paper. Two loop heat pipe systems with flat-plate evaporator were designed. The effect of a new refrigerant, R1234ze (E), on the thermal performance of the loop heat pipe was investigated. Two cooling methods were designed to achieve different cooling requirements, namely liquid-condenser and air-condenser respectively. The reliability of the solution had been fully verified. When the temperature of the heat source was kept below 75 °C, the heat load that could be cooled by the two condensing methods is 150 W (9.8 W/cm2). The largest heat load of the liquid-condenser could even reach 270 W (16.9 W/cm^2) under gravity assistance. For the air-condenser, the normal operating range was 10 W–150 W while the working power of the fan was 20 W. Under different operating conditions, the system responded quickly and without any failures. The minimum total thermal resistance of liquid-condenser LHP and air-condenser LHP was 0.307 °C/W and 0.135 °C/W, respectively. These two LHPs meet the cooling needs of electronic devices and can effectively alleviate the thermal problems of electronic devices.

1. Introduction

The loop heat pipe (LHP) is an efficient passive cooling device [1], which is widely used to cool electronic devices. In the initial stages, loop heat pipes were primarily utilized for cooling chips in the aerospace industry [2,3]. With the development of LHP and the increase of electronic equipment cooling requirements, it has become possible to apply LHP to cool electronic devices such as integrated CPU, IGBT, MOSFET, etc. With flexible installation, good cooling performance and low manufacturing cost, LHP has received wide attention. Table 1 lists the technical parameters of some mainstream electronic devices.

Cylindrical [5] and flat plate [6] were two types of evaporator shapes that were commonly used. Flat-panel packaged LHP [7] had also been widely investigated. Compared with cylindrical evaporators, flat plate evaporators have the advantages of simple installation, low thermal resistance, and can be tightly contact with the surface of the heat source. Therefore, in the field of cooling electronic equipment [8,9], most LHP evaporators were designed to be flat-shaped. For flat plate evaporators, the internal porous structures (wicks) also need to be improved and studied. Mathews et al. [10] studied the effect of the optimal sintering temperature of Cu-Ni composite wick on its hydraulic and thermal properties. Kumar et al. [11] studied the heat transfer characteristics of the bi-porous in the LHP and believed that the bi-porous influenced the cooling performance of electronic equipment. Solomon et al. [12] made a compact LHP for cooling IGBT modules, which incorporated a bio-wick. Other scholars [13–15] had also used wicks of different materials to improve the heat transfer properties of LHPs. Chen et al. [16] believed that bi-porous had better hydraulic properties, which was of great help to improve the heat transfer performance of the system.

The practical application value of LHP is an important criterion for evaluating the cooling system. For thermal management of electronic devices, factors such as cooling system material, working fluid, fin form, and installation size, need to be considered. LHP commonly used working fluids include water [17], ammonia [18,19], refrigerants [20–22], nanofluids [23,24], organic solvents [25,26], etc. Many scholars had done corresponding experimental research and built prototypes for practical application. Li et al. [27] proposed a solution to the cooling problems of LEDs. In this solution, the heat load range that the LHP could normally operate was 0–100 W. Kelvin et al. [28] designed an ultra-thin loop heat pipe, and achieve a minimum start-up heat flux of 2 W/cm^2. Shioga et al. [29,30] made an ultra-thin LHP and applied it to

* Corresponding author.
E-mail address: w_liu@hust.edu.cn (W. Liu).

https://doi.org/10.1016/j.tsep.2023.101935
Received 15 June 2022; Received in revised form 26 April 2023; Accepted 28 May 2023
Available online 2 June 2023

Nomenclature

Amb	Ambient
C	Condenser
COP	Coefficient of performance
CC	Compensation chamber
E	Evaporator
EC	Evaporator chamber
GWP	Global warming potential
HS	Heated surface
LHP	Loop heat pipe
n	Safety factor
ODP	Ozone depletion potential
Q	Heat load
R	Thermal resistance

Greek symbols

σ_1	Principal stress in the x-direction
σ_2	Principal stress in the y-direction
σ_3	Principal stress in the z-direction
σ_s	Ultimate stress of material
$[\sigma]$	Allowable stress

the LHP. Maydanik et al. [35] verified the reliability of LHP for cooling electronic devices through real server test experiments. Gravity assists [36] to cool the electronic equipment and helps to better control the surface temperature. In the thermal management of electronic devices, the cooling method of the heat sink also needs to be considered. For ground applications, the condensers are usually cooled with liquid or air. The tube-in-tube liquid condenser [37,38] is an efficient heat sink device, which can make the temperature of the condenser outlet approach the set target temperature, and can greatly improve the thermal performance of LHP. However, the disadvantage is that additional electrical equipment is required for cooling and circulation. Air-cooling [36,39,40] is an energy-saving and practical cooling method, which is widely used in the cooling process of electronic devices because of its convenient installation. However, the air-cooling methods usually cannot achieve complete cooling of the working fluid in the condenser, thus limiting the improvement of LHP performance.

A solution for cooling electronic devices was proposed in this study. R1234ze(E) was selected as the working fluid because it is environmentally friendly, non-corrosive, and has good thermodynamic properties. Since the application of R1234ze(E) in LHP is not yet widespread, the thermal performance of R1234ze(E)-LHP needs to be verified. The whole system was made of aluminum alloy to achieve the goals of light weight, low cost and good operation performance in commercialization. The solution includes two loop heat pipe systems, which were liquid-condenser LHP and air-condenser LHP respectively, to meet the needs

Table 1
Technical parameters of mainstream electronic devices [4].

Model	Designer	Process (nm)	Year	Size (mm × mm)	TDP (W)	Temperature (°C)
Threadripper PRO 5995WX	AMD	7	3, 2022	75.4 × 58.5	280	95
EPYC 7713P	AMD	7	1, 2021	58.5 × 75.4	240	–
EPYC 75F3	AMD	7	1, 2021	58.5 × 75.4	280	–
Ryzen 7 5800X	AMD	12	10, 2020	–	105	90
Xeon E7-8870	Intel	32	4, 2011	49.2 × 56.5	130	85
Xeon Gold 6138P	Intel	14	5, 2018	76.2 × 56.6	195	93
Xeon Bronze 3204	Intel	14	4, 2019	76.2 × 56.6	85	77
Xeon Platinum 8124	Intel	14	2017	76.2 × 56.6	240	–
Neoverse N1	ARM	7	2, 2019	–	100	–
EMAG 8180	TSMC	16	2, 2018	–	125	90
ThunderX2 CN9980	Cavium	16	5, 2018	–	200	–
Centriq 2460	Qualcomm	10	11, 2017	55 × 55	120	–

cool the mobile phone chips. This prototype had the largest heat load of 20 W. Zhou et al. [31] applied LHP to laptops and controlled the hot spot temperature within 96 °C while ensuring the largest heat load of 15 W. Zilio et al. [32] controlled the heat of Integrated Modular Avionics and proposed a modular cooling device using loop heat pipes. The system was tested with heat loads between 3 W and 60 W. Bernagozzi et al. [33] and Jouhara et al. [34] applied LHP to battery management and HVAC systems, respectively. These tests expanded the scope of application of of different environments and cooling objectives. The solution was designed to facilitate the use of LHP in cooling electronics. The performance of LHPs was fully tested in the experiments. The longest transmission distance of LHPs was 870 mm, which satisfied the separation arrangement of the heat source and heat sink. the largest heat load reached 270 W under the condition that the heat source temperature was kept below 75 °C. The successful validation of the thermal management solutions proposed in this study introduces a new pathway for

Table 2
Physical parameters of common working fluids.

Working fluid	Standard boiling point (°C)	Saturation pressure (20 °C, MPa)	Saturate vapor density (20 °C, kg/m^3)	Latent heat of vaporization (20 °C, kJ/kg)	Surface tension (20 °C, 10^{-3}N/m)	ODP	GWP
Ammonia	33.588	0.857477	6.7025	1186.3748	21.636	–	–
Acetone	55.690	0.024662	0.6011	539.2244	23.335	–	–
Ethanol	78.087	0.005876	0.1115	926.0101	22.411	–	–
Methanol	64.148	0.013032	0.1751	1176.5752	22.567	–	–
Pentane	35.678	0.056558	1.7248	370.1076	16.006	–	–
Water	99.605	0.002339	0.0173	2453.5193	72.736	–	–
R152a	24.318	0.512906	15.9095	285.3205	10.378	0	124
R141b	31.671	0.065023	3.2127	228.4229	18.814	0.11	630
R245fa	14.812	0.122704	7.1468	193.2505	14.279	0	790
R134a	26.361	0.571707	27.7802	182.2806	8.692	0	1430
R1233zd(E)	17.966	0.107961	6.0515	194.4461	15.200	0	7
R1234ze(E)	19.274	0.427343	22.6071	170.6264	9.499	0	6

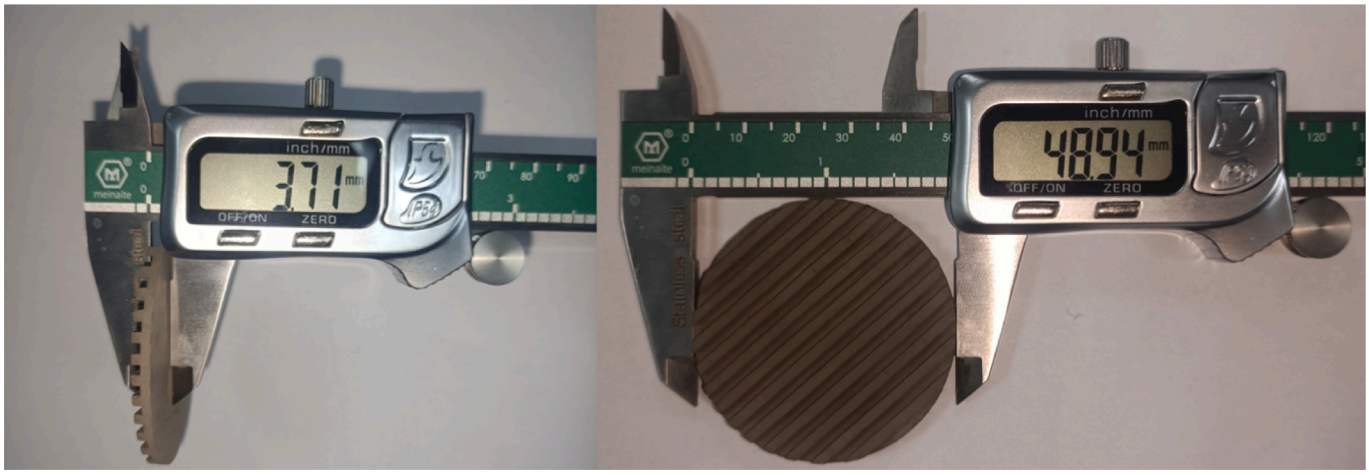

(a)

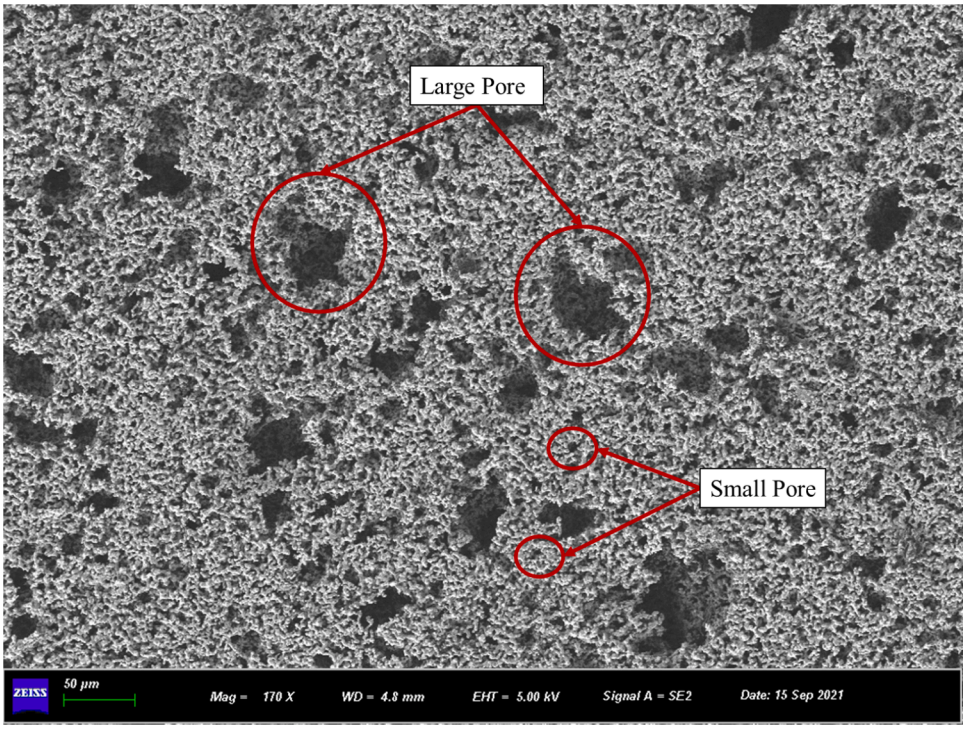

(b)

Fig. 1. Image data of the biporous wick. (a) The structural dimensions of biporous wick. (b) SEM test image at 170x magnification.

cooling electronic devices.

2. Experimental setup

2.1. Working fluid

The physical parameters of the working fluid are the key factors affecting the performance of LHP. For electronic device cooling solutions, in addition to the thermodynamic properties of the working fluid, toxicity and flammability during the application should be considered. Table 2 consists of a few common working fluids in LHP. Ammonia is a kind of effective working fluid for LHP. Due to the characteristics of low saturated boiling point and large latent heat of phase transition for the ammonia, the working performance of ammonia-LHP is characterized by a low start-up threshold, stable operation and sensitive thermal response. However, toxicity to the human body and high saturation pressure (50 °C, 2.03 MPa) are the defects that restrict the use of ammonia in cooling electronic devices. The standard boiling point of water and ethanol are 100 °C and 78.3 °C, respectively, which cannot keep the temperature of electronic devices at a low range. Methanol and acetone can also cause irreversible damage to human health, and cannot be used on a large scale in practical applications. The Global Warming Potential (GWP) and ozone depletion potential (ODP) are important indicators for evaluating the environmental friendliness of a refrigerant. R134a and R245fa have GWP values of 1430 and 790, respectively, so they are not an environmentally-friendly choice. Both R1233zd(E) and R1234ze(E) are the fourth-generation environmentally-friendly refrigerants of Honeywell, and their GWP and ODP values are at low levels. The standard boiling point of R1234ze(E) is lower than R1233zd (E), so R1234ze(E) has a lower activation threshold.

At 50 °C, the saturation pressure of R1234ze(E) is 0.99 MPa, with little mechanical damage to the system structure. The ODP and GWP

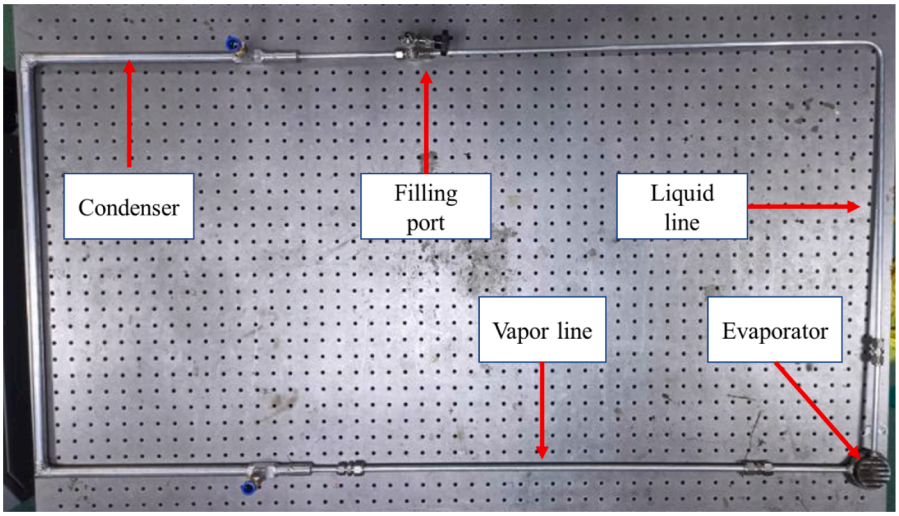

(a)

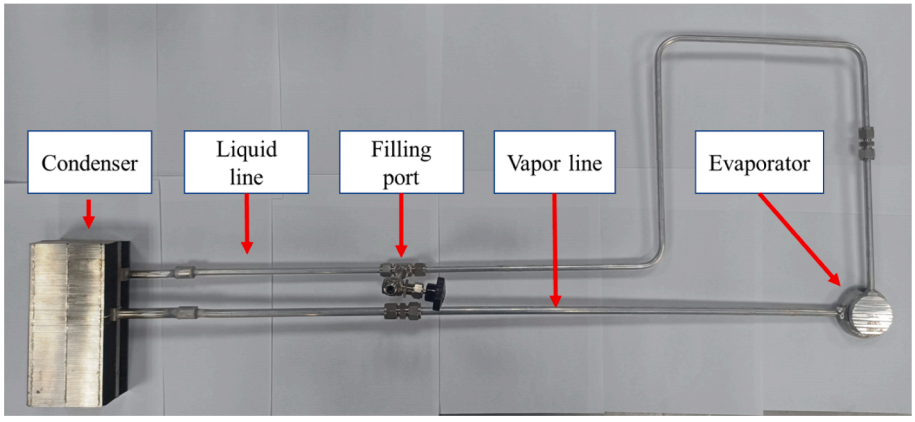

(b)

Fig. 2. Physical picture of the assembled LHPs. (a) Liquid-condenser LHP. (b) Air-condenser LHP.

values of R1234ze(E) are 0 and 6, respectively, which is an environmentally friendly working fluid that can be used for electronic device cooling. In addition, the application of R1234ze(E) in LHP was not yet widespread, and the thermal properties of R1234ze(E)-LHP need to be evaluated. Considering the above factors, R1234ze(E) was finally selected as the working fluid in this solution.

2.2. Design of the LHP

The LHP in this solution consisted of an evaporator, a condenser, and two transport lines. The evaporator was a flat vertical liquid supply design, which contained a biporous wick that drives the working fluid circulation. The biporous wick was made of nickel powder with a diameter of 2.6 μm and the sodium carbonate pore-forming agent. The manufacturing process of biporous wick mainly consisted of the following 5 steps: powder mixing, extrusion molding, sintering, pore-forming agent removal, and drying. The porosity of the biporous wick was measured by the Archimedes method. Two wicks with porosity of 74.83% and 76.26% were selected. The structural dimensions of biporous wick are shown in Fig. 1(a), and the distribution of large and small pores can be seen in the figure. The electron microscope scan of biporous wick is shown in Fig. 1(b).

The solution included two sets of LHPs, which were liquid-condenser LHP and air-condenser LHP, respectively. Two sets of LHPs were designed to meet the different needs of cooling electronic devices. The structure of the liquid-condenser was tube-in-tube. An aqueous solution of ethylene glycol was circulated in the outer pipeline of the condenser, and the temperature of the circulating medium was controlled by a thermostatic bath. Sufficient condensing capacity could be provided during system operation by tube-in-tube condensers which were easy to manufacture. This design fulfilled the need for strong condensation and easy assembly in the cooling solution of electronic devices. The air-condenser consisted of an ordinary axial fan and an efficient air heat exchange finned microchannel structure. The air at ambient temperature scoured the surface of the fins through the fan to take away the heat in the channel. The air-condenser only needed a fan to dissipate heat, which could meet the requirements of compact structure, reliability and stability in the cooling solution of electronic devices. Fig. 2 is the physical picture of the assembled LHPs. All parts of the system have been marked in the figure. The systems were placed on the optical table. The LHPs were all made of aluminum alloy to achieve light weight, low cost and easy assembly during practical application. The parameters of each component of two LHPs in this solution are shown in Table 3.

Table 3
Basic dimensions of LHPs.

		Liquid-condenser LHP	Air-condenser LHP
Evaporator	Overall height	21.8 mm	21.8 mm
	Diameter	60 mm	60 mm
	Heating area	45 mm	45 mm
	Material	T7075	T7075
Liquid line	Inner/outer diameter	6/8 mm	6/8 mm
	Length	1457 mm	1375 mm
	Material	T6061	T6061
Vapor line	Inner/outer diameter	8/10 mm	8/10 mm
	Length	815 mm	870 mm
	Material	T6061	T6061
Liquid-condenser	Inner/outer diameter of inner pipe	6/8 mm	–
	Inner/outer diameter of outer pipe	14/16 mm	–
	Length	1385 mm	–
	Material	T6061	–
Air-Condenser	Length/width/height	–	185/90/60 mm
	Material	–	T6061
Wick	Diameter	48.94 mm	48.54 mm
	Height	3.71 mm	4.01 mm
	Number of grooves	13	13
	Width/height of the groove	2 mm	2 mm
	Porosity	74.83%	76.26%
	Material	Nickel	Nickel

2.3 Structural analysis of evaporator

The evaporator is the key component in the LHP, performing the functions of heat absorption and circulation of the working fluid. The performance of the LHP could be affected by the design of the evaporator. A more application-friendly evaporator was designed in this study, which was achieved by changing the evaporator material, inlet and outlet locations, and weld seam locations. The structure of the evaporator as shown in Fig. 3 was flat, which could fit well with electronic devices and reduce thermal resistance. The design of the inlet and outlet of the evaporator was perpendicular to each other, which reduced the installation space during practical application. In addition, the biporous wick needed to be encapsulated in the evaporator to keep the liquid side separated from the vapor side, forming a compensation chamber (CC) and an evaporation chamber (EC) respectively. After encapsulating the wick, laser welding of the evaporator shell and the evaporator cover was required to ensure the airtightness of the system. The welding positions were distributed on the side of the evaporator shell.

Considering the pressure change of the working fluid and the temperature control requirements of electronic devices, a suitable evaporator was designed. The wall thickness was designed to be 2 mm to prevent mechanical damage by internal pressure. Usually, the evaporator materials were stainless steel, copper, etc. The aluminum alloy is a good conductor of heat because its thermal conductivity is 230 W/m•K, which is greater than that of stainless steel. Thus, the use of aluminum alloy could reduce the thermal resistance between the evaporator and the electronic devices. At the same time, the aluminum alloy has good compatibility and does not react physical and chemical reactions with R1234ze(E). The yield strength of aluminum alloy can reach 503 MPa, which has a stronger pressure resistance ability than copper. The saturation pressure of R1234ze(E) is 0.99 MPa at 50 °C, and the aluminum alloy fully satisfies the safety requirements. Therefore, the aluminum alloy was chosen for evaporator materials.

Before the evaporator structure was applied to this solution, a numerical analysis of structural strength was required. The maximum deformation and minimum safety factor when the structure was subjected to the maximum pressure needed to be analyzed. For the strength check of the evaporator structure, three assumptions were defined:

(1) The evaporator material was a continuous, uniform, isotropic elastic medium;
(2) The pressure was evenly applied to each surface in the evaporator;
(3) The contact surface between the pipe and the evaporator as the fixed surface was selected.

The failure criteria are as follows:

$$\sqrt{\frac{1}{2}\left[(\sigma_1-\sigma_2)^2+(\sigma_1-\sigma_3)^2+(\sigma_2-\sigma_3)^2\right]}\leqslant[\sigma] \tag{1}$$

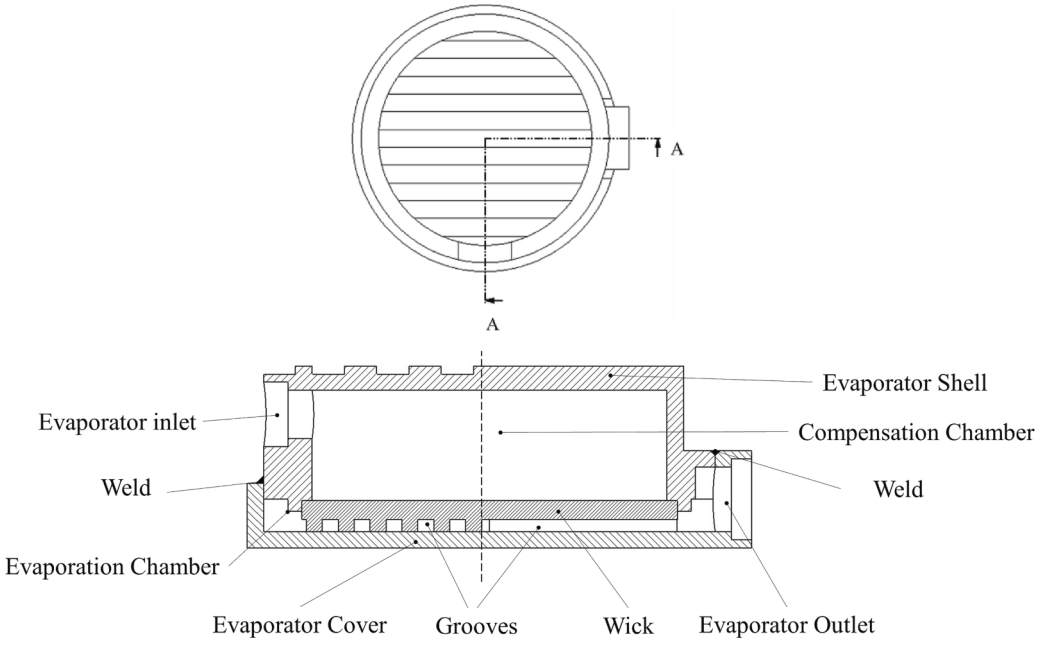

Fig. 3. Schematic diagram of evaporator structure.

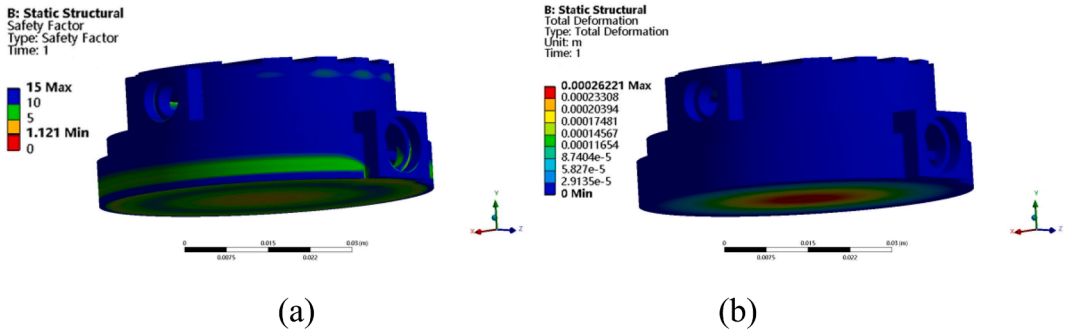

Fig. 4. Structural analysis of the evaporator. (a) Safety factor. (b) Total deformation.

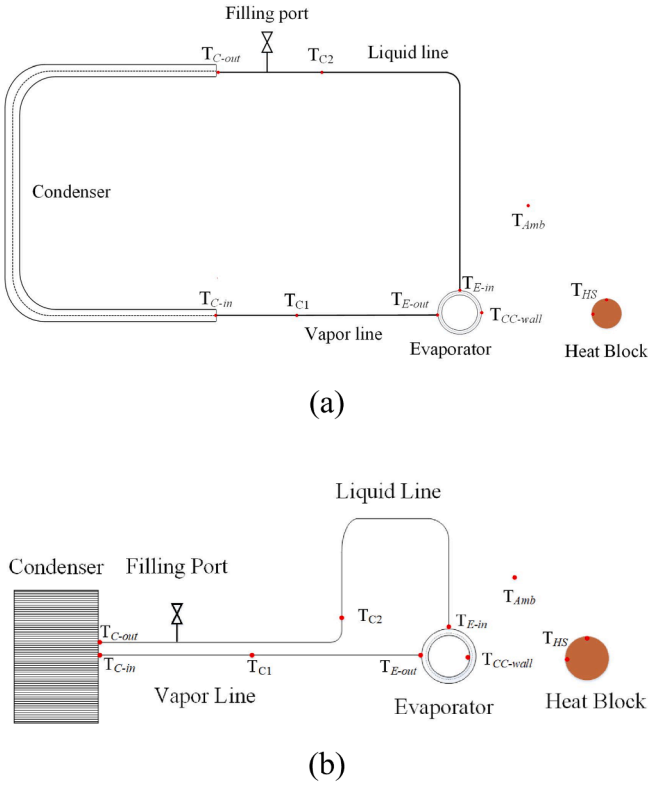

Fig. 5. Thermocouple distribution of the system. (a) Liquid-condenser LHP. (b) Air-condenser LHP.

$$n = \frac{\sigma_s}{[\sigma]} \tag{2}$$

where σ_1, σ_2, σ_3 are three kinds of principal stresses, $[\sigma]$ is allowable stress, σ_s is the ultimate stress of the material, n is the safety factor. The safety factory is an important indicator for evaluating structural safety. The structural design is safe when the safety factor is greater than or equal to 1.

During the numerical calculation, Ansys 2020R1 was used for the structural analysis of the evaporator. When the vapor temperature of R1234ze(E) was 50 °C, the corresponding saturation pressure was 0.99 MPa. In order to replicate the stress environment under the operation of LHPs, a consistent pressure of 1 MPa was uniformly exerted on the inner wall of the evaporator. The cloud diagrams of the safety factor and total deformation distribution are shown in Fig. 4. From Fig. 4(a), it can be proved that most of the structural safety factor of the evaporator is higher than 5. The minimum value of the safety factor of the entire evaporator was 1.121, ensuring the safety of the system during operation. The maximum deformation of the evaporator is 0.26 mm, which is located in the center of the evaporator cover.

2.4. Test methods

During the experiment, the temperature of each part was measured in real time through thermocouples. The thermocouple distributions are shown in Fig. 5. The T-type thermocouples were used in the experiment, and the absolute error was ±0.5 K after calibration. The temperature data collector was sampled at an interval of 3 s, and the collected data were recorded in a PC.

A smooth copper block was used as a simulated heat source. Four heating rods with a diameter of 6 mm were embedded into the bottom of the copper block to ensure sufficient heating power. The working conditions of the LHPs were changed by adjusting the output power of the power supply.

The liquid-condenser LHP used a thermostatic bath to control the heat sink temperature. The circulating medium in the thermostatic bath was an aqueous solution of ethylene glycol prepared at a ratio of 1:1. Two ordinary fans with a speed of 4600 RPM were adopted in the air-condenser LHP, and the size of the fans was 12 × 12 × 3 cm. The fans were powered by DC 12 V 2.7 A and were installed with a power output regulator. The wind speed and wind temperature were monitored in real time by the hot-wire anemometer.

Before charging, the system was pumped into a vacuum to decrease the influence of the non-condensable gas. The two LHPs were connected to a vacuum pump and vacuumed to 3×10^{-4} Pa. The charging ratio of the liquid-condenser LHP and the air-condenser LHP were 62.7% and 65.9%, respectively.

3. Results and discussions

In order to verify the reliability of the solution to the cooling problem of electronic devices, test experiments under start-up, variable heat load, and gravity assist were designed. At the same time, the characteristic temperature of the system and the thermal resistance of LHPs were analyzed.

3.1. Liquid-condenser LHP

3.1.1. Start-up

Start-up performance is one of the important indicators of LHP. The heat sink temperatures in the test were −10, 5, and 20 °C, respectively. The heat source temperature was kept below 75 °C, and the liquid-condenser LHP was placed horizontally. Fig. 6 shows the lowest heat load start-up curves for the three heat sink temperatures of the liquid-condenser LHP. During the experiment, The lowest heat load at all three heat sink temperatures was 10 W. The lowest heat load start-up process was divided into two stages, which were the overshoot stage and the equilibrium stage. During the overshoot phase, most of the heat transferred from the heated surface was absorbed by the sensible heat of

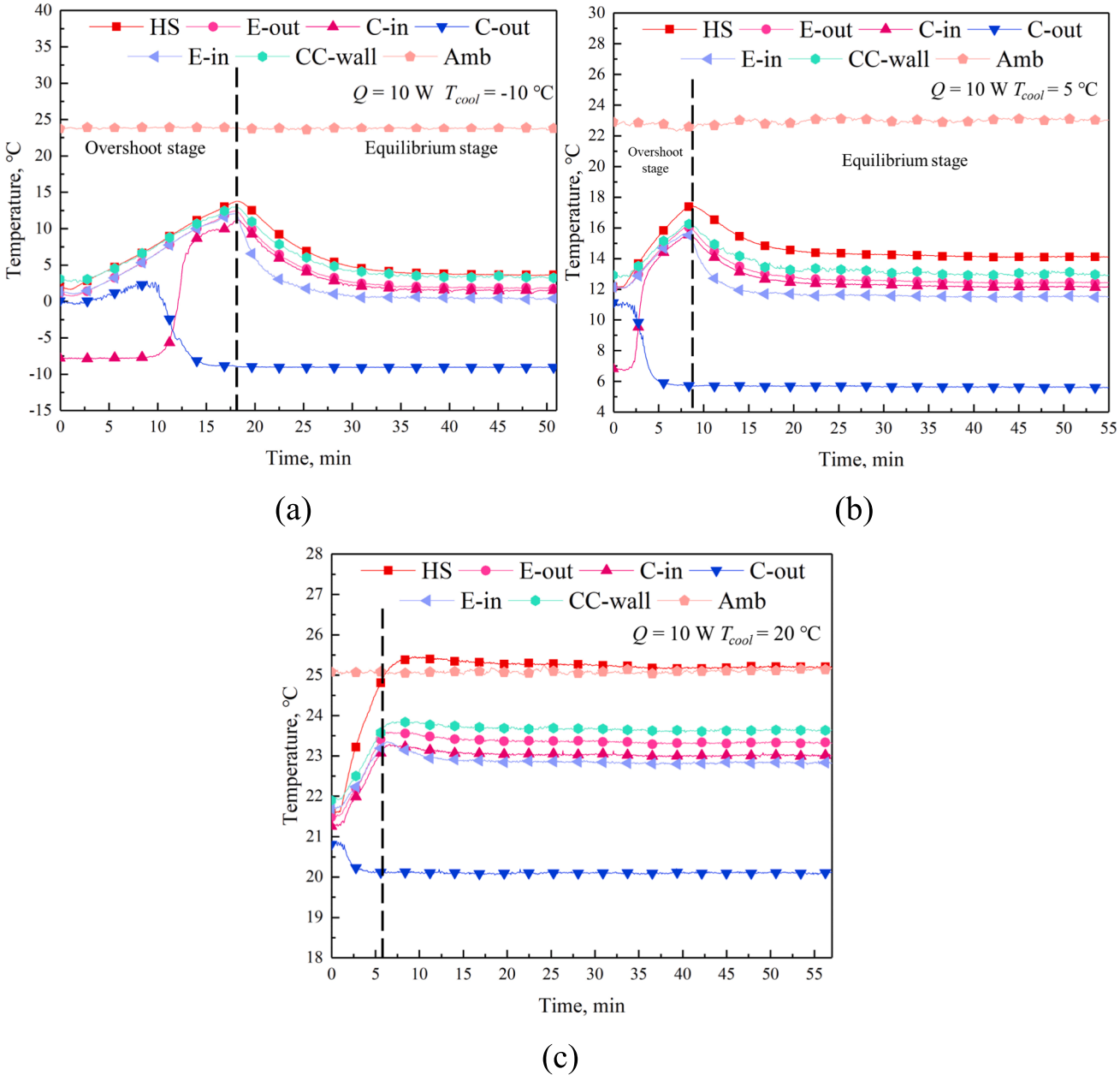

Fig. 6. 10 W start-up curves with various heat sink temperatures. (a) −10 °C. (b) 5 °C. (c) 20 °C.

the working fluid. The remaining heat leakage was transferred to the CC, which caused the evaporator temperature to rise. The working fluid in the EC was gradually vaporized and accumulated, which pushed the liquid in the vapor line toward the condenser. The circulating working fluid carried away the heat from the EC and brought enough subcooled fluid to the CC. The subcooled fluid in the CC absorbed the leaked heat. As the heat sink temperature grew up, the temperature overshoot value decreased. This phenomenon was due to the temperature increase of the liquid in the pipeline, which reduced the heat required for vaporization and affected the time spent in this stage. The time required for the overshoot stage at the three heat sink temperatures was 17, 8.5, and 6 min, respectively. In the equilibrium stage, the vapor-liquid distribution in each part of the system was stable, and the system circulation was successfully established. The evaporator shell was made of aluminum alloy, and the thermal conductivity was about 230 W/m•K which had the strong ability of temperature uniformity, so the inlet and outlet temperatures of the evaporator were similar.

The largest heat load is shown in Fig. 7. The corresponding largest heat loads under the three heat sink temperature conditions were 150, 110, and 80 W, respectively. During the largest heat load star-up test, the temperature of the heated surface did not exceed 75 °C, and the vapor temperature was set to be within 50 °C. The largest heat load was 150 W, corresponding to a heat flux of 9.8 W/cm^2. A large amount of heat was absorbed by the evaporator in a short time, and the working fluid in the EC rapidly vaporized and formed the superheated vapor. The pressure differential that existed between the condenser and evaporator drove the movement of the working fluid. The temperature of the system was stabilized when the capillary force, the vapor drive force and the flow resistance were balanced. During the test, the system could be started within 20 min, and the temperature of the heat source could be accurately controlled.

The heat leakage was absorbed by the sensible heat of the liquid in the CC, which was an important heat transfer method under low heat load conditions. Therefore, the CC temperature was higher than the

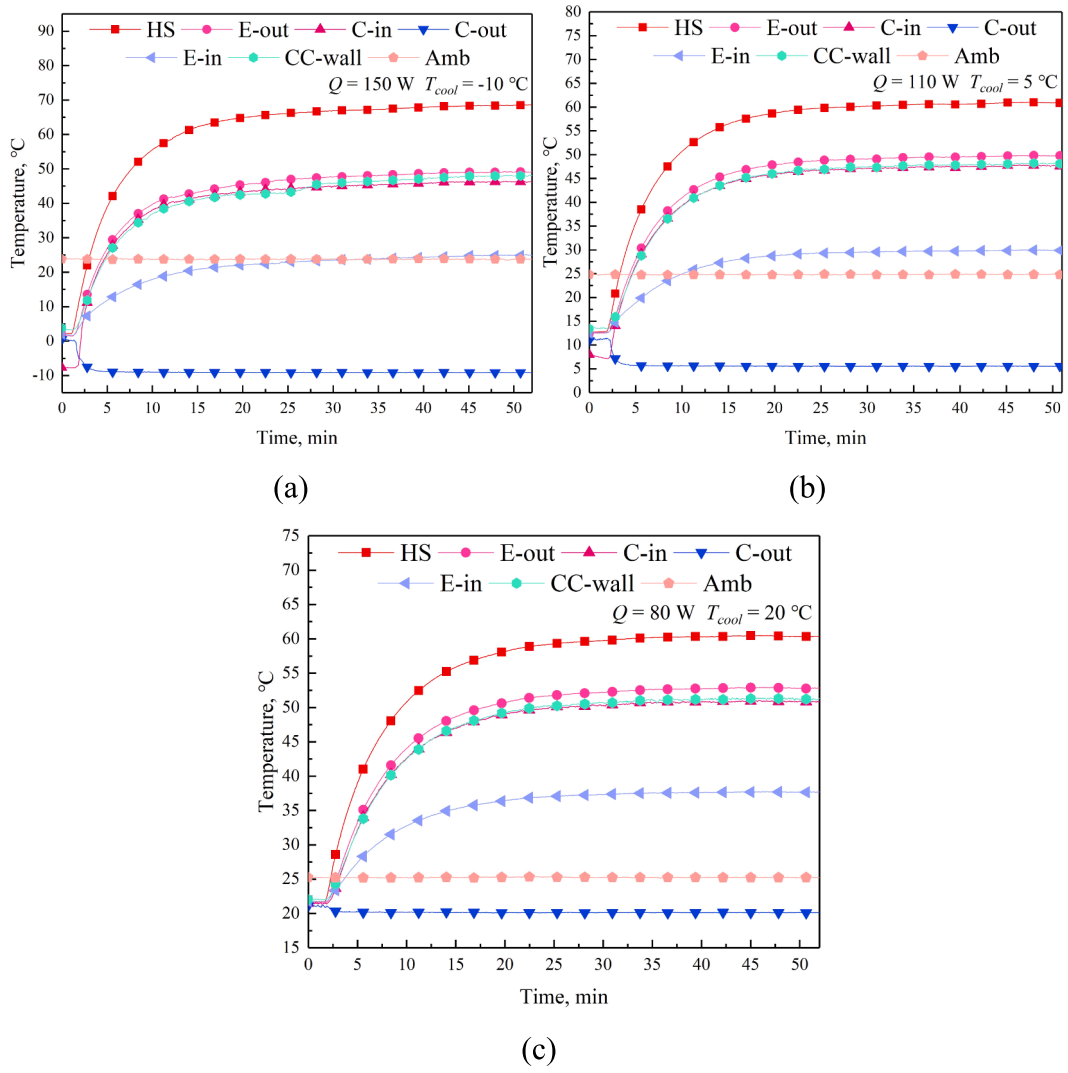

Fig. 7. Largest heat load with different heat sink temperatures. (a) −10 °C, 150 W. (b) 5 °C, 110 W. (c) 20 °C, 80 W.

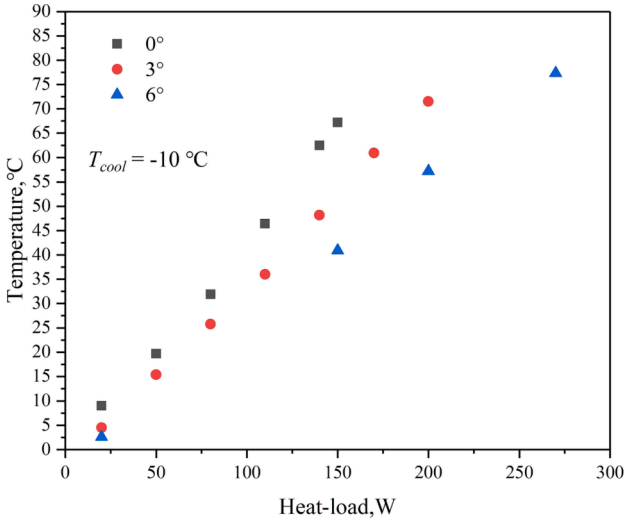

Fig. 8. System thermal performance at different inclination angles.

evaporator outlet temperature. As the heat load increased, more of the heat in the EC was taken away by vapor, and the proportion of heat transferred through heat leaks decreases. Therefore, the evaporator outlet temperature was higher than CC under high heat load conditions.

3.1.2. *Gravity assist*

In practical application, the installation inclination angle of the LHP should be arranged according to the space of the electronic device. When the installation height of the evaporator and the condenser was not horizontal, the gravity assist could change the performance of the system. During the test, the system heat sink temperature was −10 °C, and the system inclination angles were changed to 3° and 6°, respectively. Fig. 8 is a graph of the thermal performance test for the largest heat load at three inclination angles of the test system. The condenser was installed above the evaporator with an inclination angle, and the driving force of the working fluid circulation was increased. The reflux liquid could better enter the CC, which reduced the heat leakage problem in CC, and the wick was completely wetted. The gravity head due to the height difference increased the pressure inside the CC and prevented the vapor in the EC from leaking to the CC. Therefore, with the increase of the inclination angle, the heat transfer capacity of the system was significantly enhanced. For every 3° increase in the inclination angle of the liquid-condenser lhp, the performance of the system could have been improved by 33.3%-35%. At 3° and 6° inclination, the largest heat load

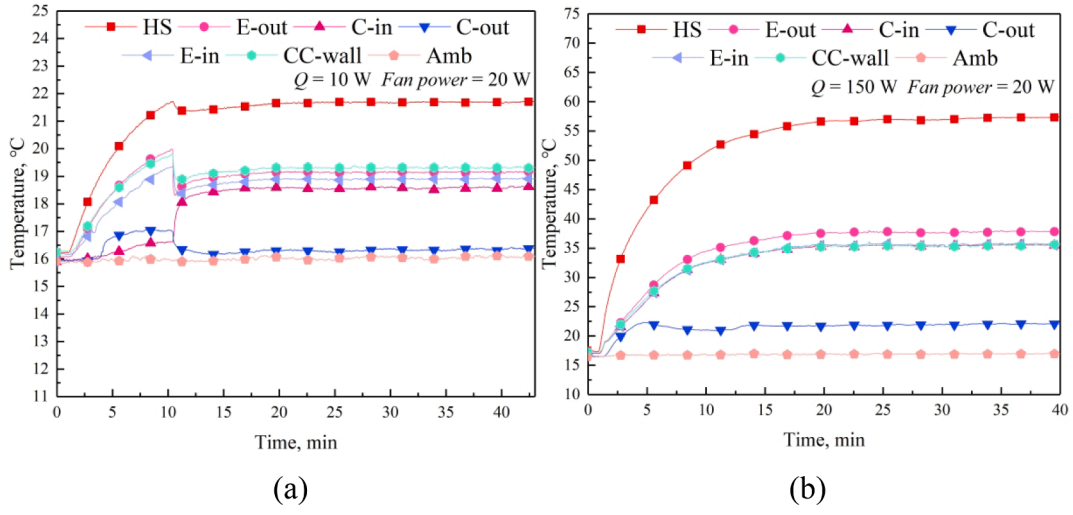

Fig. 9. Air-condenser LHP start-up performance. (a) Q = 10 W. (b) Q = 150 W.

was 200 W (12.6 W/cm^2) and 270 W (16.9 W/cm^2), respectively, and it could fully meet the cooling problems of electronic devices with different heat load and installation spaces.

3.2. Air-condenser LHP

3.2.1. Start-up

Forced air cooling was used in the air-condenser LHP. The performance of the air-condenser was affected by the ambient temperature. The ambient temperature in this experiment was about 16 °C. Under this experimental condition, the fan power was set to 20 W. The lowest and largest start-up heat loads of the air-condenser LHP were 10 W and 150 W respectively, as shown in Fig. 9. Compared with the liquid-condenser LHP, the air-condenser LHP could achieve the same heat load condition, and the working capacity of the condenser could fully meet the system cooling requirements. When starting under the low heat load, the circulating speed of the working fluid was slow in the overshoot stage, and the condenser did not effectively reduce the temperature of the vapor, thus the condenser outlet temperature rose slowly. This phenomenon disappeared with the end of the system overshoot phase. After reaching the equilibrium stage, the temperature of the system was stable and there were no fluctuations in the outlet temperature of the condenser. The heat exchange capacity of the air-condenser had reached equilibrium. Under the condition of high heat load, the vapor circulation speed was fast and the circulation amount was stable after 5 min, so the outlet temperature of the condenser could be quickly stabilized. Overall, the temperature fluctuation phenomenon could be equilibrated within 12 min for the initial stage of the air-condenser startup, which was very useful for the timely cooling of the electronic device. When the heat load was 150 W (9.8 W/cm^2), the heated surface temperature was 57 °C. There was no temperature overshoot phenomenon during start-up, and the system worked stably.

The air-condenser LHP performed well at ambient temperature, and exhibited the ability to cool 150 W of heat load with a fan power input of 20 W. The system had high cooling efficiency with a *COP* value of 7.5. The COP value is defined by the following equation:

$$COP = \frac{P_{heat}}{P_{input}} \tag{3}$$

where *COP* is the coefficient of performance, P_{heat} is the heat load of the evaporator, and P_{input} is the fan input power.

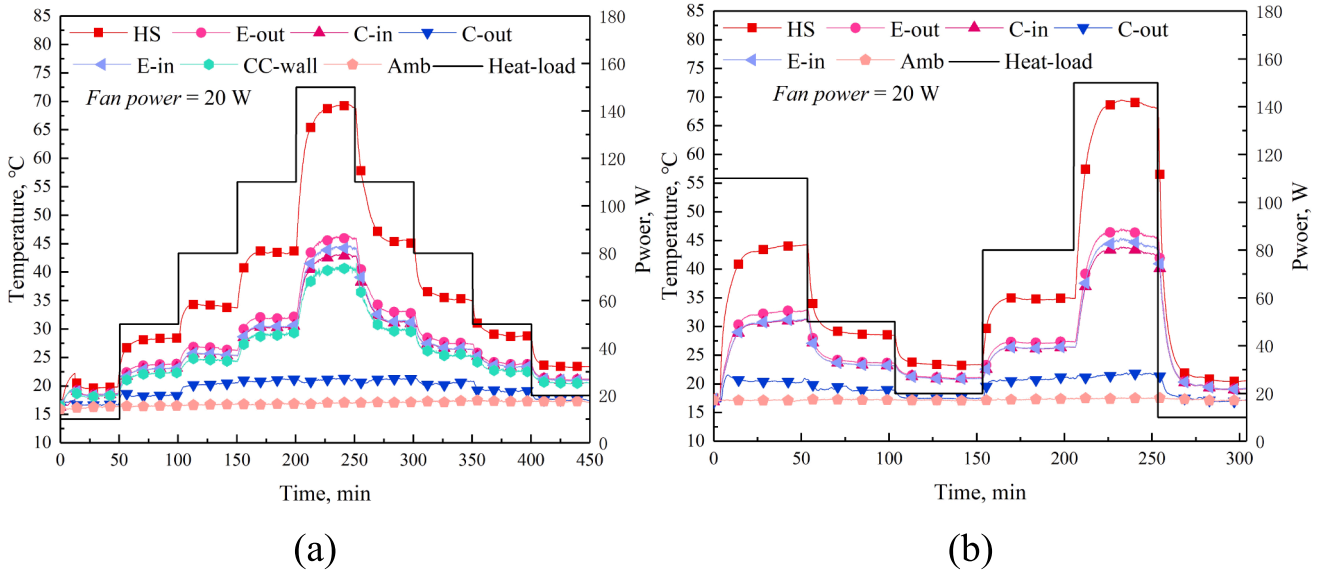

Fig. 10. Air-condenser LHP variable heat load performance curve. (a) Step-variable heat load. (b) Random-variable heat loads.

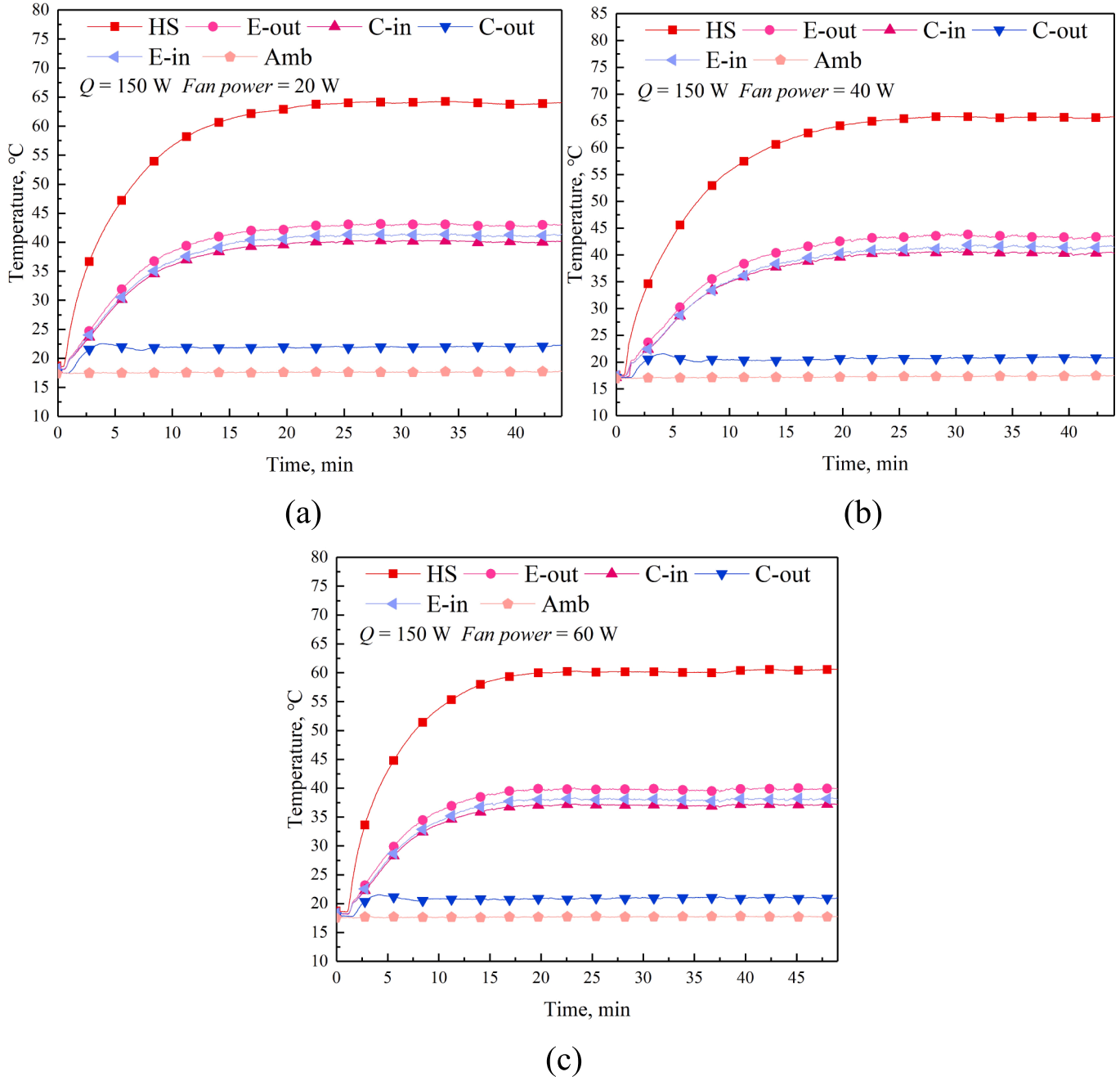

Fig. 11. System thermal performance under three kinds of fan power with the heat load of 150 W. (a) 20 W. (b) 40 W. (c) 60 W.

3.2.2. *Variable heat load*

Electronic devices operate under non-rated power and unstable conditions, then the waste heat generated is different. Therefore, variable thermal load conditions are a frequently encountered operating condition for electronic equipment. In this experiment, the step-variable heat load and random-variable heat load processes of LHP were tested to simulate the unsteady cooling process of electronic devices. The working conditions were adjusted every 50 min, and the trend of the heat load in the step-variable heat load test was to increase first and then decrease. In the random-variable heat load test, the heat load was randomly adjusted to deal with the random working conditions of electronic devices. Fig. 10 shows the thermal performance curves of the air-condenser LHP for step-variable heat load and random-variable heat load. The heated surface temperature was kept below 75 °C, and the heat loads varied from 10 W to 150 W. The air-condenser LHP could respond quickly in a short time when the heat load changed. There was no phenomenon that the temperature of the heated surface was uncontrollable. Fig. 10(a) shows that the condenser outlet temperature does not fluctuate when the heat load was higher than 80 W, and the condenser outlet temperature could even approach ambient temperature under low heat load conditions. The condenser could ensure sufficient condensation during the cooling process of electronic devices. In the falling stage of the heat load, the vapor–liquid distribution in the system and the heat load state of the front stage were different from those in the rising stage. Part of the wick was evaporated to dryness, and vapor was present in the CC due to heat leakage. Therefore, the thermal performance of the air-condenser LHP was worse in the falling stage of the heat load than in the rising stage, which would affect the precise temperature control of the electronic devices. When the heat load was 110 W, the difference between the rising and falling stage of the temperature of the heated surface was

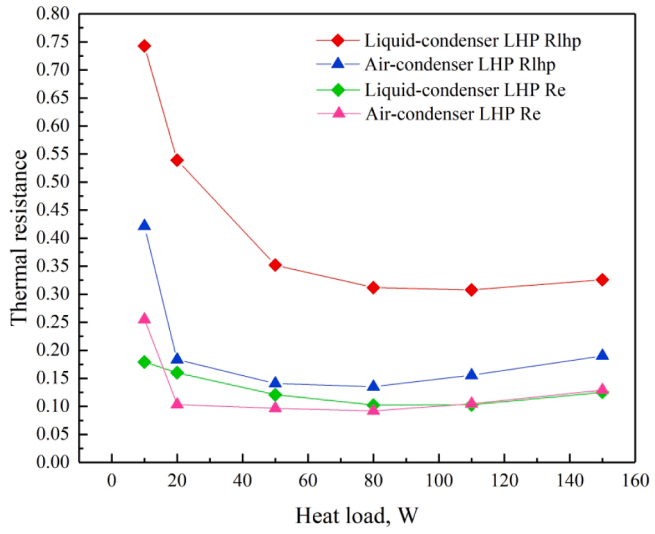

Fig. 12. Thermal resistance versus heat load for two systems.

2 °C. When the heat loads were 80 W and 50 W, the difference was 1.3 and 0.4 °C respectively. Fig. 10(b) is the test curve of the random-variable heat load. The air-condenser LHP could always achieve state transition within 15 min when the heat load changed. The cooling solution could solve the thermal problem of any electronic device with a thermal design power of 150 W.

3.2.3. *Variable fan power*

Improving the heat exchange efficiency of the condenser is an effective temperature control method for the air-condenser LHP. In the experiment, the fan power was changed to improve the heat transfer coefficient of the condenser. In the test, the fan power was 20, 40 and 60 W respectively. The value of the wind speed and temperature through the condenser was collected via a hot-wire anemometer. During the test, the heat load of 150 W was applied and the system was placed horizontally. The thermal performance curves under three fan powers are shown in Fig. 11. The corresponding operating temperatures of the three fan powers were 67.8, 62.9, and 60.5 °C, respectively. When the fan power was 60 W, the outflow wind speed of the condenser was 9 m/s. As the fan power increased, the condensation efficiency increased by 8% and 2% respectively. Under three different fan powers, the air temperatures leaving the condenser were 27.4 °C, 25.5 °C, and 25 °C, respectively. The air-condenser LHP had a limited impact on the thermal performance of the system by changing the different fan powers. The air-condenser LHP had a strong stability in the process of cooling electronic equipment.

3.3. *The characteristic temperature and thermal resistance analysis*

Evaporator thermal resistance and LHP thermal resistance are important parameters to characterize the heat transfer performance of the system, which are determined by the following formulas:

$$R_E = \frac{T_{HS} - T_{E-out}}{Q} \tag{4}$$

$$R_{LHP} = \frac{T_{HS} - T_C}{Q} \tag{5}$$

where R_E is the evaporator thermal resistance, R_{LHP} is the total thermal resistance of the system, T_{HS} is the heated surface temperature, $T_{E\text{-}out}$ is the evaporator outlet temperature, T_C is the average temperature of the condenser, and Q is the heat load. R_E was usually related to the contact between the evaporator and the heated surface, the flow state in the EC, and the tight assembly of the wick and the shell. Considering the practical application of the LHP, a series of measures had been taken to reduce the R_E value, such as changing the structure of the evaporator, designing the welding position on the side of the shell, and filling the gap between the heated surface and the evaporator with high thermal conductivity silicone grease.

Table 4
Uncertainties of the parameter.

Parameters	Nomenclature	Uncertainty
Temperature	ΔT	0.5 K
Liquid-condenser LHP R_E	$\Delta R/R$	3.27%
Liquid-condenser LHP R_{LHP}	$\Delta R/R$	1.34%
Air-condenser LHP R_E	$\Delta R/R$	3.17%
Air-condenser LHP R_{LHP}	$\Delta R/R$	2.17%
Output voltage	$\Delta U/U$	0.17%
Output current	$\Delta I/I$	0.47%
Output power	$\Delta Q/Q$	0.5%

Fig. 12 shows a thermal resistance comparison between the two systems. Under the condition of low heat load, the evaporation rate of the working fluid in the EC increased, and the phase change of the working fluid in the wick only occurred on the surface, so the thermal resistance value decreases. Under the condition of high heat load, the liquid in the EC completely evaporated and formed a stable gas film, so the thermal resistance increased instead. The minimum thermal resistance of the evaporators of the two systems was 0.102 °C/W and 0.092 °C/W respectively, and the minimum values both occurred when the heat load was 80 W. The minimum total thermal resistance of liquid-condenser LHP and air-condenser LHP was 0.307 °C/W and 0.135 °C/W, respectively.

The formulas in the literature [41] were used to calculate the uncertainty of each parameter. The calculation results are shown in Table 4.

Fig. 13 shows the relationship between the operating temperature and the thermal load of the two LHPs. The temperature control capability of the liquid-condenser LHP under different heat loads is shown in Fig. 13(a). The temperature of the heated surface increased linearly with the increase of the heat load, which could realize the precise temperature control of the heated surface temperature. It could be seen from Fig. 13(b) that the fluctuation of ambient temperature affected the working performance of the air-condenser LHP, especially in the case of low heat load. The evaporator shell was made of aluminum alloy with strong temperature uniformity. For the air-condenser LHP, the difference between each temperature measurement point on the evaporator was within 3 °C. Under high heat load conditions, the thermal resistance values of the two LHP systems were similar, and the heat transfer performance was alike. And because the ambient temperature of the air-condenser LHP was lower than the ambient temperature of the liquid-condenser LHP under the test conditions, the heat in the CC was more likely to be transferred to the environment, resulting in different temperature behavior under high heat load conditions.

4. Conclusions

In this study, two sets of flat-plate loop heat pipes were proposed to solve the cooling problem of electronic devices. A practical evaporator structure and manufacturing scheme were designed. The thermal performance of the system was tested using experimental methods. The conclusions are as follows:

(1) All components of the two systems were made of aluminum alloy to meet the practical requirements of light weight and low cost. The compatibility and reliability of aluminum alloy and R1234ze (E) had been proved by experimental tests.
(2) The heated surface temperature was kept below 75 °C. The transmission distance of the liquid-condenser LHP was 815 mm, the normal operating range was 10–150 W (0.63–9.8 W/cm^2) at

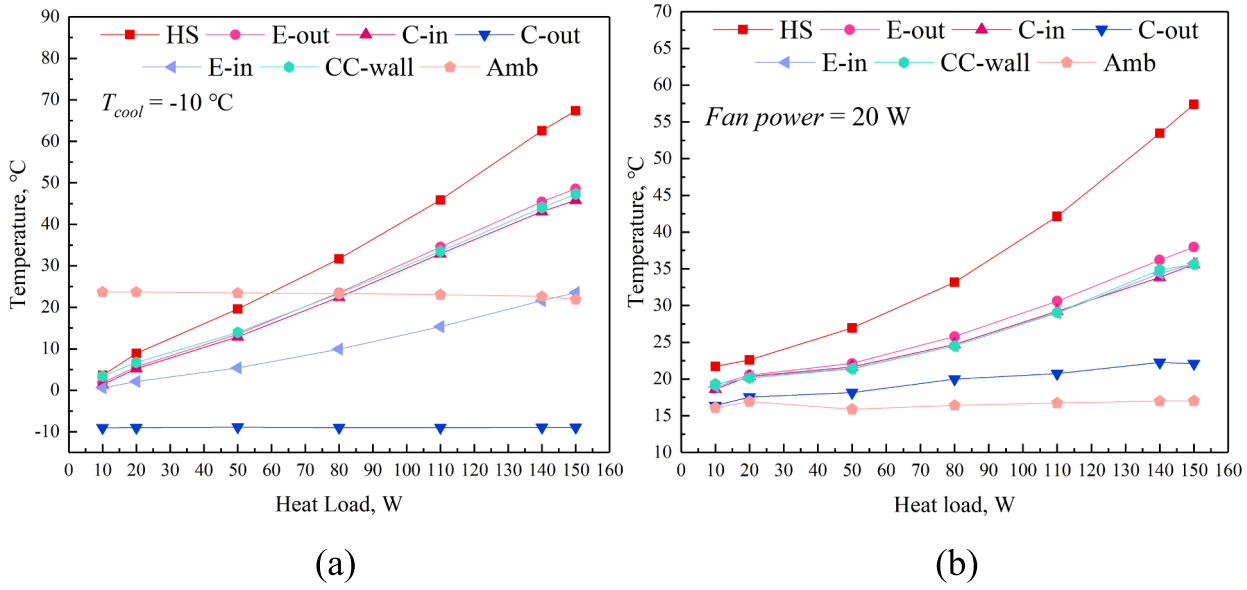

Fig. 13. System operating temperature versus heat load. (a). Liquid-condenser LHP. (b). Air-condenser LHP.

−10 °C, and the largest heat load could reach 270 W (16.9 W/cm^2) with the 6° inclination.

(3) The air-condenser LHP had the largest heat load of 150 W at ambient temperature and the *COP* value was 7.5. The air-condenser had good performance under various working conditions, and there was no abnormal temperature fluctuation during the test.

(4) Both sets of LHPs showed good heat transfer performance under all heat load conditions. At 80 W, the evaporator thermal resistance and total thermal resistance value were minimized. The minimum thermal resistance was 0.092 °C/W.

CRediT authorship contribution statement

S.C. Zhao: Conceptualization, Methodology, Software, Validation, Formal analysis, Investigation, Data curation, Writing – original draft, Writing – review & editing, Visualization. **Zikang Zhang:** Methodology, Software, Writing – review & editing. **Runze Zhao:** Methodology, Software, Formal analysis. **Tong Wu:** Methodology, Writing – review & editing. **Xiaoyu Zhang:** Conceptualization, Funding acquisition. **Z.C. Liu:** Conceptualization, Writing – review & editing, Resources, Supervision, Project administration, Funding acquisition. **Wei Liu:** Conceptualization, Writing – review & editing, Resources, Supervision, Project administration, Funding acquisition.

Declaration of Competing Interest

The authors declare that they have no known competing financial interests or personal relationships that could have appeared to influence the work reported in this paper.

Data availability

No data was used for the research described in the article.

Acknowledgements

This work was supported by the National Natural Science Foundation of China (No. 52076088) and the Foundation of State Key Laboratory of Coal Combustion (FSKLCCA2007).

References

[1] Y.F. Maydanik, Loop heat pipes, Appl. Therm. Eng. 25 (2005) 635–657.
[2] Y. Guo, G. Lin, H. Zhang, J. Miao, Investigation on thermal behaviours of a methane charged cryogenic loop heat pipe, Energy 157 (2018) 516–525.
[3] Y.n. Zhao, N. Wang, T. Yan, J. Liang, H. Chen, Experimental study on operating characteristics of a cryogenic loop heat pipe without additional power consumption, Appl. Therm. Eng., 184 (2021).
[4] WikiChip, WikiChip. https://en.wikichip.org/wiki/WikiChip 2013, (accessed 2022).
[5] M.A. Chernysheva, Y.F. Maydanik, Simulation of heat and mass transfer in a cylindrical evaporator of a loop heat pipe, Int. J. Heat Mass Transf. 131 (2019) 442–449.
[6] Y.F. Maydanik, S.V. Vershinin, M.A. Chernysheva, Experimental study of an ammonia loop heat pipe with a flat disk-shaped evaporator using a bimetal wall, Appl. Therm. Eng. 126 (2017) 643–652.
[7] Z. Chen, X. Tong, H. Liu, C. Guo, F. Qu, H. Cong, A design of the Micro-Plate Loop Heat Pipe and development of the porous nickel capillary wick, Procedia Eng. 205 (2017) 3931–3937.
[8] S. Du, Q. Zhang, P. Hou, C. Yue, S. Zou, Experimental study and steady-state model of a novel plate loop heat pipe without compensation chamber for CPU cooling, Sustain. Cities Soc. 53 (2020).
[9] J. Li, G. Zhou, T. Tian, X. Li, A new cooling strategy for edge computing servers using compact looped heat pipe, Appl. Therm. Eng. 187 (2021).
[10] A. Joseph Mathews, S. Ranjan, A. Inbaoli, C.S. Sujith Kumar, S. Jayaraj, Optimization of the sintering parameters of a biporous copper-nickel composite wick for loop heat pipes, Mater. Today:. Proc. 46 (2021) 9297–9302.
[11] P. Kumar, B. Wangaskar, S. Khandekar, K. Balani, Thermal-fluidic transport characteristics of bi-porous wicks for potential loop heat pipe systems, Exp. Therm. Fluid Sci. 94 (2018) 355–367.
[12] A.B. Solomon, A.K. Mahto, R.C. Joy, A.A. Rajan, D.A. Jayprakash, A. Dixit, A. Sahay, Application of bio-wick in compact loop heat pipe, Appl. Therm. Eng. 169 (2020).
[13] Z. Hu, D. Wang, J. Xu, L. Zhang, Development of a loop heat pipe with the 3D printed stainless steel wick in the application of thermal management, Int. J. Heat Mass Transf. 161 (2020).
[14] S.-C. Wu, T.-J. Lee, W.-J. Lin, Y.-M. Chen, Study of self-rewetting fluid applied to loop heat pipe with PTFE wick, Appl. Therm. Eng. 119 (2017) 622–628.
[15] Y. Yamada, M. Nishikawara, H. Yanada, Y. Ueda, Predicting the performance of a loop heat pipe considering evaporation from the meniscus at the three-phase contact line, Therm. Sci. Eng. Progr. 11 (2019) 125–132.
[16] B.B. Chen, Z.C. Liu, W. Liu, J.G. Yang, H. Li, D.D. Wang, Operational characteristics of two biporous wicks used in loop heat pipe with flat evaporator, Int. J. Heat Mass Transf. 55 (2012) 2204–2207.
[17] Y. Maydanik, S. Vershinin, M. Chernysheva, S. Yushakova, Investigation of a compact copper–water loop heap pipe with a flat evaporator, Appl. Therm. Eng. 31 (2011) 3533–3541.
[18] F. Qu, H. Liu, C. Jiang, C. Guo, Y. Liu, C. Zhang, Nickel-ammonia loop heat pipe based on the molten salt pore forming startup and heat transfer failure characteristics of experimental study, Procedia Eng. 205 (2017) 3938–3945.
[19] N.S. Ramasamy, P. Kumar, B. Wangaskar, S. Khandekar, Y.F. Maydanik, Miniature ammonia loop heat pipe for terrestrial applications: Experiments and modeling, Int. J. Therm. Sci. 124 (2018) 263–278.

[20] H. Jouhara, H. Ezzuddin, Thermal performance characteristics of a wraparound loop heat pipe (WLHP) charged with R134A, Energy 61 (2013) 128–138.
[21] H. Wang, G. Lin, L. Bai, Y. Tao, D. Wen, Comparative study of two loop heat pipes using R134a as the working fluid, Appl. Therm. Eng. 164 (2020).
[22] R. Zhao, Z. Zhang, S. Zhao, H. Cui, Z. Liu, W. Liu, Experimental study of flat-disk loop heat pipe with R1233zd(E) for cooling terrestrial electronics, Appl. Therm. Eng. 197 (2021).
[23] H.R. Goshayeshi, M. Goodarzi, M.R. Safaei, M. Dahari, Experimental study on the effect of inclination angle on heat transfer enhancement of a ferrofluid in a closed loop oscillating heat pipe under magnetic field, Exp. Therm. Fluid Sci. 74 (2016) 265–270.
[24] P. Gunnasegaran, M.Z. Abdullah, N.H. Shuaib, Influence of nanofluid on heat transfer in a loop heat pipe, Int. Commun. Heat Mass Transfer 47 (2013) 82–91.
[25] A.R. Anand, A. Ambirajan, P. Dutta, Investigations on vapour blanket formation inside capillary wick of loop heat pipe, Int. J. Heat Mass Transf. 156 (2020).
[26] A.R. Anand, A. Jaiswal, A. Ambirajan, P. Dutta, Experimental studies on a miniature loop heat pipe with flat evaporator with various working fluids, Appl. Therm. Eng. 144 (2018) 495–503.
[27] J. Li, F. Lin, D. Wang, W. Tian, A loop-heat-pipe heat sink with parallel condensers for high-power integrated LED chips, Appl. Therm. Eng. 56 (2013) 18–26.
[28] K.G. Domiciano, L. Krambeck, J.P.M. Flórez, M.B.H. Mantelli, Thin diffusion bonded flat loop heat pipes for electronics: Fabrication, modelling and testing, Energ. Conver. Manage. 255 (2022).
[29] T. Shioga, T. Abe, H. Nagano, Submillimeter-thick loop heat pipes fabricated using two-layer copper sheets for cooling electronic applications, Appl. Therm. Eng. 181 (2020).
[30] T. Shioga, Y. Mizuno, H. Nagano, Operating characteristics of a new ultra-thin loop heat pipe, Int. J. Heat Mass Transf. 151 (2020).
[31] G. Zhou, J. Li, Z. Jia, Power-saving exploration for high-end ultra-slim laptop computers with miniature loop heat pipe cooling module, Appl. Energy 239 (2019) 859–875.
[32] C. Zilio, G. Righetti, S. Mancin, R. Hodot, C. Sarno, V. Pomme, B. Truffart, Active and passive cooling technologies for thermal management of avionics in helicopters: Loop heat pipes and mini-Vapor Cycle System, Therm. Sci. Eng. Progr. 5 (2018) 107–116.
[33] M. Bernagozzi, A. Georgoulas, N. Miché, C. Rouaud, M. Marengo, Novel battery thermal management system for electric vehicles with a loop heat pipe and graphite sheet inserts, Appl. Therm. Eng. 194 (2021).
[34] H. Jouhara, R. Meskimmon, An investigation into the use of water as a working fluid in wraparound loop heat pipe heat exchanger for applications in energy efficient HVAC systems, Energy 156 (2018) 597–605.
[35] Y.F. Maydanik, S.V. Vershinin, M.A. Chernysheva, Investigation of thermal characteristics of a loop heat pipe in a wide range of external conditions, Int. J. Heat Mass Transf. 147 (2020).
[36] K. Odagiri, H. Nagano, Heat transfer characteristics of flat evaporator loop heat pipe under high heat flux condition with different orientations, Appl. Therm. Eng. 153 (2019) 828–836.
[37] C. Han, L. He, Z. Tian, B. Xu, Z. Chen, Study of heat dissipation characteristics of loop heat pipe with heat sink of composite material, Appl. Therm. Eng. 200 (2022).
[38] W. Ling, W. Zhou, R. Liu, Z. Shen, C. Liu, J. Huang, Experimental investigation of loop heat pipe with novel interlaced microchannel condenser, Int. Commun. Heat Mass Transfer 125 (2021).
[39] J. Li, D. Wang, G.P. Peterson, Experimental studies on a high performance compact loop heat pipe with a square flat evaporator, Appl. Therm. Eng. 30 (2010) 741–752.
[40] Z.-P. Wan, X.-W. Wang, Y. Tang, Condenser design optimization and operation characteristics of a novel miniature loop heat pipe, Energ. Conver. Manage. 64 (2012) 35–42.
[41] R.J. Mofat, Describing the uncertainties in experimental results, Exp. Therm. Fluid Sci. 1 (1988) 3–17.